

Primary and Secondary Flows on Unsteady MHD Free Convective Micropolar Fluid Flow Past an Inclined Plate in a Rotating System: a Finite Element Analysis

M. D. Shamshuddin^{1,*} and P. V. Satya Narayana²

Abstract: In the present paper, a numerical analysis is performed to study the primary and secondary flows of a micropolar fluid flow past an inclined plate with viscous dissipation and thermal radiation in a rotating frame. A uniform magnetic field of strength B_0 is applied normal to the plane of the plate. The whole system rotates with uniform angular velocity about an axis normal to the plate. The governing partial differential equations are transformed into coupled nonlinear partial differential equations by using the appropriate dimensionless quantities. The resulting equations are then solved by the Galerkin finite element method. The influencing pertinent parameters like primary and secondary velocities, primary and secondary angular velocities, temperature and concentration profiles are represented with the help of graphs. The validity and accuracy of finite element code is benchmarked with the results reported in the literature under some limiting cases. The study is relevant to rotating MHD (magnetohydrodynamics) energy generators utilizing non-Newtonian working fluids and magnetic rheo-dynamic materials processing systems.

Keywords: Thermal radiation, viscous dissipation, secondary flow, Micropolar fluid, Galerkin finite element method, rotating system.

Nomenclature

B_0	applied magnetic field strength
C_f	skin friction coefficient
C_{fx}	primary skin friction coefficient
C_{fy}	secondary skin friction coefficient
C_m	wall couple stress
C_p	specific heat at constant pressure $J Kg^{-1}K^{-1}$

¹ Department of Mathematics, Vaagdevi College of Engineering (Autonomous), Warangal, Telangana, India.

² Department of Mathematics, SAS, Vellore Institute of Technology, Vellore, Tamil Nadu, India.

*Corresponding author: M. D. Shamshuddin. Email: shammaths@gmil.com.
mdshamshuddin@vaagdevieng.ac.in.

C_s	concentration susceptability $mol\ m^{-3}$
C_w	concentration of the solute at the plate $mol\ m^{-3}$
C_{w_x}	primary wall couple stress
C_{w_y}	secondary wall couple stress
C_{w_x}	primary wall couple stress
C_{w_y}	secondary wall couple stress
C_∞	free stream concentration $mol\ m^{-3}$
D_m	molecular diffusivity $m^2\ s^{-1}$
Ec	Eckert number
F	Radiative-conduction parameter
g	acceleration due to gravity ms^{-1}
G_m	solutal Grashof number
G_r	Grashof number
j^*	Micro inertia coefficient
K	Permeability parameter
Kr	chemical reaction parameter
n	Non-dimensional oscillation frequency
Nu	Nusselt number
p	constant pressure
Pr	Prandtl number
q_r	radiative heat flux [$W\ m^{-2}$]
Q	heat source parameter
R	rotation parameter
Re_x	local Reynolds number
S	suction parameter
Sc	Schmidt number
Sh_x	Sherwood number
t	dimensionless time
T	temperature of the field in the boundary layer [K]
T_w	wall temperature of the fluid K
T_∞	temperature of the fluid in free stream K
U_r	uniform reference velocity
u, v	primary and secondary velocities
x'	axis along the plate m
y'	axis perpendicular to the plate m

Greek symbols

α	inclination angle
Δ	microrotation parameter
β_T	volumetric coefficient of concentration expansion K^{-1}
β_C	volumetric coefficient of concentration expansion K^{-1}
ρ	density of micropolar fluid $kg\ m^{-3}$
κ	thermal conductivity $Wm^{-1}K^{-1}$
k^*	mean absorption coefficient m^{-1}
σ	electrical conductivity of the fluid $s\ m^{-1}$
σ^*	Stefan-Boltzmann constant $Wm^{-2}K^{-4}$
ν	Kinematic viscosity m^2s^{-1}
ν_r	Kinematic vortex viscosity $m^2\ s^{-1}$
μ	fluid dynamic viscosity
λ	coefficient of gyro-viscosity $kg\ m^{-1}s^{-1}$
γ	gyroscopic viscosity
Ω	constant uniform angular
ε	small quantity
θ	dimensionless temperature
ϕ	dimensionless concentration
ψ	shape function
ω_1	primary angular velocity
ω_2	secondary angular velocity

1 Introduction

Over recent years, a wide range of study has been carried out on several fluid models to characterize the real fluid behaviour. One such fluid is micropolar fluid. The basic idea of micropolar fluid has risen from the need to model many engineering processes involving non-Newtonian fluids containing micro-constituents such as blood flow, lubricants, colloidal fluids, liquid crystals and suspension fluids that cannot be described by the classical Newtonian fluid. The micro-elements in micropolar fluids are of dumbbell shaped and may sustain both rotary and translation motions, as elucidated by Eringen [Eringen (1966)]. Generally, each micro-element of micropolar fluid possesses six degrees of freedom (three corresponding to translation and three corresponding to rotation). So, the micropolar theory has been able to explain many phenomena at micro and nano scales. Numerous studies of the theory and its applications have been done by many researchers. Comprehensive reviews of the subject and its applications can be found in the review articles by Ariman et al. [Ariman, Turk and Sylvester (1973, 1974)] and the books by Lukaszewicz [Lukaszewicz (1999)].

Investigation of hydromagnetic natural convection micropolar flow in a rotating medium is of considerable importance due to large applications in various areas such as rotary compressors, rotating heat exchangers, multi stage cyclone separators, astrophysics as well as in nuclear power reactors. Rotating fluid system produces two types of flows, they are Coriolis force and centrifugal force. Entire theory of rotating fluid describes the balance between Coriolis force and viscous force at the boundaries. Since Coriolis force induces motion in secondary flow direction and micropolar fluid cannot sustain a simple shearing motion, where only one component of velocity is present. The interest in the present new problem generates from the importance of studying both primary and secondary flow when the boundaries are subjected to slow rotation which can be seen in Iynger et al. [Iynger and Geeta vani (2004)], Beg et al. [Beg, Ghosh and Narahari (2010)], Kendoush [Kendoush (2013)], Maqbool et al. [Maqbool, Ayesha, Idreesa et al. (2016)]. Radiative heat transfer effects of a rotating fluid are highlighted in Mbeledogu et al. [Mbeledogu and Ogulu (2007)]. Gosh et al. [Gosh, Beg and Narahari (2007)] also highlighted the heat transfer characteristics in a rotating system with Hall effects. The rotationally symmetric flow of micropolar fluid in a rotating disk was studied by Nazir et al. [Nazir, Hussain and Shafique (2015)]. Bakr [Bakr (2011, 2013)] inspected the flow of micropolar fluid with oscillatory plate velocity in rotating frame of reference. Recently, Satya Narayana et al. [Satya Narayana, Venkateswarlu and Venkataramana (2013)] computed Hall current and radiation absorption effects for micropolar fluid in a rotating frame of reference. Anika et al. [Anika, Hoque and Islam (2013)] also computed Hall current effects on rotating vertical porous plate. Rehman [Rehman, Imran Khan, Sadiq et al. (2017)] examined MHD flow of a carbon micropolar nanofluid with convective heat transfer in a rotating frame. Tetbirt [Tetbirt, Bouaziz and Taher Abbas (2016)] showed numerically the magnetic effect on velocity distribution in macro/micro scale for both viscous and micropolar fluids.

At high temperatures, radiation effects can be quite substantial because the radiative flows of an electrically conducting micropolar fluid in the presence of magnetic field are encountered in many engineering applications such as solar power technology, nuclear engineering, electric power generating and many other industrial applications. In recent years, free convection micropolar fluid flow with radiative, heat absorbing and chemically reacting heat transfer with oscillatory plate velocity have mobilized some interest, for instance Modather et al. [Modather, Rashad and Chamkha (2009)] presented an analytical study of oscillatory flow of a micropolar fluid with heat and mass transfer effects. Das [Das (2011)] conducted a valuable analytical study for micropolar fluid in a rotating frame of reference with chemical reaction and thermal radiation effects. Pal et al. [Pal and Talukdar (2012)] studied analytically mixed convection periodic flow of a micropolar fluid considering chemical reaction and thermal radiation effects. Similar studies on micropolar fluid with different heat and mass transfer conditions has been studied by the many researches such as, Olajuwon et al. [Olajuwon and Oahimire (2013)] with thermal radiation and thermo-diffusion effects, Chaudhary et al. [Chaudhary and Preeti (2014)] with Hall current, variable suction, Soret effect in slip flow regime, Kundu, Das et al. [Das and Jana (2015)] with thermal radiation and thermal diffusion effects, Bakr et al. [Bakr and Chamkha (2017)] with variable heat flux and thermal radiation effects, Shamshuddin et al. [Shamshuddin and Thumma (2017)] with Soret and Dufour

effects. Cross diffusion effects with higher order chemical reaction effects on micropolar fluid was examined by Arifuzzaman et al. [Arifuzzaman, Rana, Ahmed et al. (2017)]. Seth et al. [Seth, Ansari and Nandkeolyar (2011)], Seth et al. [Seth, Nandkeolyar and Ansari (2013)], Seth et al. [Seth, Sarkar and Hussain (2014)] with Newtonian heating and rotations effects, rotating micropolar fluid with variety of configurations was presented by Sheikholeslami et al. [Sheikholeslami, Hatami and Ganji (2014)], Gibanov et al. [Gibanov, Sheremet and Pop (2016)], Raza et al. [Raza, Azizah and Omar (2016)].

In the most of investigations, the viscous dissipation term is conventionally neglected on the premise that under normal conditions the Eckert number is small based on an order of magnitude analysis. However, in certain materials fabrication operations, viscous dissipation can exert a prominent role. Viscous dissipation effects on the lubrication characteristics of micropolar fluids were examined by Khonsari et al. [Khonsari and Brewe (1994)]. Abdelkhalek [Abdelkhalek (2008)] discussed the radiation and dissipation effects on micropolar fluid with time dependent suction. Siva Reddy et al. [Siva Reddy and Shamshuddin (2015)] have presented numerical solutions for coupled heat and mass transfer in magnetohydrodynamic micropolar flow with both viscous dissipation and chemical reaction effects. Siva Reddy et al. [Siva Reddy and Shamshuddin (2016)] have further presented finite element numerical solutions for diffuso-thermal and chemical reaction effects on transient free convection micropolar flow. Recently, Hayat et al. [Hayat, Farooq, Ahmed et al. (2016)], Hayat et al. [Hayat, Sajjad, Ellahi et al. (2017)] subsequently analysed peristaltic flow of micropolar fluid with Newtonian heating over curved channel under the influence of heat source/sink and chemical reaction effects. Jeffery fluid flow over stretching sheet with Joule heating effects, power law heat flux was examined by Babu et al. [Babu and Satya Narayana (2016)]. Casson fluid over a moving wedge filled with gyrotactic microorganism was examined by Raju et al. [Raju, Hoque and Sivasankar (2016)]. Carreau nanofluid over a cone packed with alloy nanoparticles was examined by Raju et al. [Raju, Hoque, Anika et al. (2017)]. Casson fluid flow dispersion over radiative vertical cylinder was examined by Reddy et al. [Reddy, Reddy and Kumar et al. (2018)]. Micropolar nanofluid flow over stretching sheet with non-uniform heat source/sink was studied by Pal et al. [Pal and Mondal (2017)]. Miroshnichenko et al. [Miroshnichenko, Sheremet and Pop (2017)] examined the effect of local heat source in a micropolar fluid filled in tepezoidal cavity. Thripathy et al. [Thripathy, Dash, Mishra et al. (2016)] studied hydromagnetic micropolar fluid along a stretching sheet. Thumma et al. [Thumma, Beg and Kadir (2017)] studied numerically nano fluid flow from a non-linear inclined stretching/shrinking sheet and more recently, Baag et al. [Baag, Mishra and Hoque (2018)] studied MHD boundary layer flow over exponentially stretching sheet. Reddy [Reddy (2015)] with steady convective slip flow under uniform heat and mass flux in presence of thermal radiation, chemical reaction, ohmic heating and heat source. Anika et al. [Anika and Hoque (2013)] investigated the influence of Hall and ion slip currents on developed flow. Further, Anika et al. [Anika, Hoque, Hossain et al. (2015)] studied the impact of thermal diffusion on micropolar fluid flow with Hall and ion slip currents. More recently, Hussain et al. [Hussain, Jain, Seth et al. (2017)] demonstrated the effects of Hall current, heat absorption and chemical reaction past moving plate in a rotating system.

Motivated by the above investigations, a mathematical model is presented to study the primary as well as secondary flows of a micropolar fluid flow past an inclined porous plate in the presence of viscous dissipation and thermal radiation. In the present study, we generalized and extended the existing works of Bakr [Bakr (2011, 2013)], Das [Das (2011)] and Bakr et al. [Bakr and Chamkha (2017)] in two directions. (i) To consider the both primary and secondary flows in the model and (ii) To solve the equations by widely accepted and robust Galerkin finite element technique instead of the perturbation approximate. The effect of various physical parameters on the translational velocity, micro-rotation velocity, temperature and concentration profiles as well as on local skin friction coefficient, wall couple stress, Sherwood number and Nusselt number are tabulated. The current study is relevant to high temperature electromagnetic rheological flows in energy generators and magneto-rheological materials fabrication systems (where thermal radiation heat transfer is also significant) and has not appeared in technical literature thus far. The formulation and methodology of present problem is presented in Sections 2 and 3 respectively. Results and discussions are explored scientifically in Section 4. Important new findings are summarized in the conclusions Section.

2 Mathematical formulation

We considered the problem of unsteady free convective flow of an electrically conducting incompressible micro-polar fluid past an inclined plate (with inclination angle α to the vertical). The plate as well as fluid is rotating with uniform angular velocity Ω about z^* -axis in micropolar saturated porous medium. Initially at time $t^* \leq 0$ both the plate and fluid are at rest and are maintained at a uniform temperature T_∞^* and uniform surface concentration C_∞^* . At time $t^* \geq 0$, the plate starts non-torsional oscillation in its own plane in x^* direction with velocity $U_r(1 + \varepsilon \cos n^* t^*)$, the plate is maintained with uniform temperature T_w^* and concentration C_w^* . A homogeneous chemical reaction of first order with constant rate K'_r is supposed to exist between diffusing species of the fluid. The physical configuration is illustrated in Fig. 1. Darcy law is assumed for porous medium documented in Batchelor [Batchelor (1967)]. Since the magnetic Reynolds number of the flow is taken to be very small, the induced magnetic field is neglected (see Cowling [Cowling (1957)]) so that magnetic field $B = (0, B_0, 0)$. It is also assumed that no external electric field is applied so the electric field due to polarization of charges is negligible (see Seth et al. [Seth and Sarkar (2015)], Seth et al. [Seth and Singh (2013)] ($E = (0, 0, 0)$)) which corresponds that applied or polarized voltage is neglected so that no energy is added or extracted from the fluid by electrical means. Radiative heat flux is described by using Rosseland approximation. The radiative heat flux in the x^* direction is considered negligible in comparison with that of z^* direction. Ohmic (Joule) dissipation is ignored. The magnetic micropolar fluid contains a species which is reactive and obeys first order chemical reaction. Except pressure all physical quantities depend on

The energy equation:

$$\frac{\partial T}{\partial t^*} + w^* \frac{\partial T}{\partial z^*} = \left(\alpha^* + \frac{16 \sigma^* T_\infty^3}{3 k^* \rho C_p} \right) \frac{\partial^2 T}{\partial z^{*2}} - \frac{Q^*}{\rho C_p} (T - T_\infty) + \frac{\mu}{\rho C_p} \left(\frac{\partial u^*}{\partial z^*} \right)^2 \quad (6)$$

The concentration equation

$$\frac{\partial C}{\partial t^*} + w^* \frac{\partial C}{\partial z^*} = D_m \frac{\partial^2 C}{\partial z^{*2}} - K' r (C - C_\infty) \quad (7)$$

The following spatial and temporal boundary conditions are prescribed:

$$t^* \leq 0: \left\{ \begin{array}{l} u^* = v^* = 0, \quad \bar{\omega}_1^* = \bar{\omega}_2^* = 0, T = T_\infty, C = C_\infty. \\ \\ u^* = U_r \left[1 + \frac{\varepsilon}{2} \left(e^{in^* t^*} + e^{-in^* t^*} \right) \right], v^* = 0, \bar{\omega}_1^* = -\frac{1}{2} \frac{\partial v^*}{\partial z^*}, \\ \\ \bar{\omega}_2^* = \frac{1}{2} \frac{\partial u^*}{\partial z^*}, T = T_w, C = C_w \quad \text{at } z^* = 0 \\ \\ u^* \rightarrow 0, v^* \rightarrow 0, \bar{\omega}_1^* \rightarrow 0, \bar{\omega}_2^* \rightarrow 0, T \rightarrow T_\infty, C \rightarrow C_\infty \quad \text{as } z^* \rightarrow \infty \end{array} \right. \quad (8)$$

Here u^*, v^* and $\bar{\omega}_1^*, \bar{\omega}_2^*$ are the velocity and microrotation velocities along x^*, y^* directions. ν, ν_r are the kinematic and microrotational viscosities. k is the thermal conductivity, α^* is the thermal diffusivity of the fluid defines as $\alpha^* = \kappa / \rho C_p$. ρ is the density of the micropolar fluid and μ is the viscosity and β_T, β_C are the volumetric thermal and concentration coefficients. g is acceleration due to gravity, $\sigma^* (= 5.67 \times 10^{-8} \text{ W/m}^2\text{K}^4)$ is the Stefan-Boltzmann constant and k^* (m^{-1}) is the Rosseland mean absorption coefficient. C_p is the specific heat at constant pressure, Q^* is additional heat source and D_m is the mass diffusivity of species of the fluid, σ is the electrical conductivity of the micropolar fluid, γ is gyroscopic viscosity of micropolar fluid and j^* is micro inertia density and U_r is the uniform reference velocity and ε is a small quantity. The oscillatory plate velocity assumed in Eq. (8) is based on Ganapathy [Ganapathy (1994)], Integrating the continuity Eq. (1) for variable transpiration (lateral mass flux) velocity normal to the plate, a convenient solution emerges as:

$$w^* = -w_0 \quad (9)$$

Where w_0 is the normal velocity at the plate $w_0 > 0$ for suction, $w_0 < 0$ for blowing and $w_0 = 0$ corresponds to an impermeable plate and the radiative heat flux expression in Eq. (6) is given by Rosseland approximation (see Modest [Modest (1992)]) as

$$q_r = \frac{-4\sigma^*}{3k^*} \left(\frac{\partial T^4}{\partial z^*} \right) \quad (10)$$

Using Taylor’s series expansion about T_∞ the expansion of T^4 can be written as follows,

$$T^4 = T_\infty^4 + 4T_\infty^3(T - T_\infty) + 6T_\infty^2(T - T_\infty)^2 + \dots \tag{11}$$

Neglecting higher order terms beyond the first degree in $(T - T_\infty)$, we have

$$T^4 \cong 4T_\infty^3 T - 3T_\infty^4 \tag{12}$$

Now differentiating (10) w. r. t. the coordinate z^* and invoking Eq. (11), we get:

$$\frac{\partial q_r}{\partial z^*} = - \left(\frac{16\sigma^*}{3k^*} \right) T_\infty^3 \frac{\partial^2 T}{\partial z^{*2}} \tag{13}$$

Substituting T^3 in Eq. (10) with T_∞^3 , Eq. (6) can then be expressed as follows

$$\rho C_p \left(\frac{\partial T}{\partial t^*} + w^* \frac{\partial T}{\partial z^*} \right) = \left(\kappa + \frac{16\sigma^*}{3k^*} T_\infty^3 \right) \frac{\partial^2 T}{\partial z^{*2}} - Q^* (T - T_\infty) + \mu \left(\frac{\partial u^*}{\partial z^*} \right)^2 \tag{14}$$

It is pertinent to note that if this assumption is neglected, the radiative heat flux in Eq. (6) results in a highly non-linear expression (see Brewster et al. [Brewster (1992); Cortell (2008)]).

Introducing the following non-dimensional variables and parameters

$$\left. \begin{aligned} z &= \frac{z^* U_r}{\nu}, u = \frac{u^*}{U_r}, v = \frac{v^*}{U_r}, t = \frac{t^* U_r^2}{\nu}, n = \frac{n^* \nu}{U_r^2}, \omega_1 = \frac{\bar{\omega}_1^* \nu}{U_r^2}, \\ \omega_2 &= \frac{\bar{\omega}_2^* \nu}{U_r^2}, \theta = \frac{T - T_\infty}{T_w - T_\infty}, \phi = \frac{C - C_\infty}{C_w - C_\infty}, M = \frac{\sigma B_0^2 \nu}{\rho U_r^2}, \\ R &= \frac{2\Omega \nu}{U_r^2}, Gr = \frac{\nu g \beta_T (T_w - T_\infty)}{U_r^3}, Gm = \frac{\nu g \beta_C (C_w - C_\infty)}{U_r^3}, \\ S &= \frac{w_0}{U_r}, Pr = \frac{\mu \rho C_p}{\kappa}, Sc = \frac{\nu}{D_m}, F = \frac{16 T_\infty^3 \sigma^*}{3 \kappa k^*}, Q = \frac{Q^* \nu^2}{\kappa U_r^2}, \\ Ec &= \frac{U_r^2}{C_p (T_w - T_\infty)}, K = \frac{\kappa U_r^2}{\nu^2}, Kr = \frac{K' r \nu}{U_r}, \Delta = \frac{K}{\rho \nu}, \\ \lambda &= \frac{\gamma}{\mu j^*} = \left(1 + \frac{\Delta}{2} \right) \end{aligned} \right\} \tag{15}$$

Where all quantities without * are dimensionless, θ is dimensionless temperature function, ϕ is dimensionless concentration and Δ is the Eringen micropolar vortex viscosity parameter. Using dimensionless variables (15) into Eqs. (1-7) yield the following dimensionless partial differential equations

$$\frac{\partial u}{\partial t} - S \frac{\partial u}{\partial z} - Rv = (1 + \Delta) \frac{\partial^2 u}{\partial z^2} + Gr \theta \cos \alpha + Gm \phi \cos \alpha - \left(M + \frac{1}{K} \right) u - \Delta \frac{\partial \omega_2}{\partial z} \tag{16}$$

$$\frac{\partial v}{\partial t} - S \frac{\partial v}{\partial z} + Ru = (1 + \Delta) \frac{\partial^2 v}{\partial z^2} - \left(M + \frac{1}{K} \right) v + \Delta \frac{\partial \omega_1}{\partial z} \quad (17)$$

$$\frac{\partial \omega_1}{\partial t} - S \frac{\partial \omega_1}{\partial z} = \lambda \frac{\partial^2 \omega_1}{\partial z^2} \quad (18)$$

$$\frac{\partial \omega_2}{\partial t} - S \frac{\partial \omega_2}{\partial z} = \lambda \frac{\partial^2 \omega_2}{\partial z^2} \quad (19)$$

$$\frac{\partial \theta}{\partial t} - S \frac{\partial \theta}{\partial z} = \frac{1}{Pr} (1 + F) \frac{\partial^2 \theta}{\partial z^2} - \frac{Q}{Pr} \theta + Ec \left(\frac{\partial u}{\partial z} \right)^2 \quad (20)$$

$$\frac{\partial \phi}{\partial t} - S \frac{\partial \phi}{\partial z} = \frac{1}{Sc} \frac{\partial^2 \phi}{\partial z^2} - Kr \phi \quad (21)$$

Dimensionless initial and boundary conditions are

$$\left. \begin{aligned} \text{for } t \leq 0: & \left\{ \begin{aligned} u = v = 0 \quad \omega_1 = \omega_2 = 0 \quad \theta = 0, \phi = 0 \\ u = 1 + \frac{\varepsilon}{2} (e^{int} + e^{-int}) \quad v = 0, \\ \text{for } t > 0: & \left\{ \begin{aligned} \omega_1 = -\frac{1}{2} \frac{\partial v}{\partial z}, \omega_2 = \frac{1}{2} \frac{\partial u}{\partial z}, \theta = 1, \phi = 1 & \text{at } z = 0 \\ u \rightarrow 0, v \rightarrow 0, \omega_1 \rightarrow 0, \omega_2 \rightarrow 0, \theta \rightarrow 0, \phi \rightarrow 0 & \text{as } z \rightarrow \infty \end{aligned} \right. \end{aligned} \right\} \end{aligned} \right\} \quad (22)$$

The local skin friction factor

$$C_f = \frac{\tau_w^*}{\rho U_r^2} = \frac{(Cf_x + Cf_y)}{\rho U_r^2}, \text{ where}$$

$$Cf_x = \left((\mu + K) \frac{\partial u^*}{\partial z^*} + K \omega_1^* \right)_{z^*=0} = \rho U_r^2 \left[(1 + \Delta) \frac{\partial u}{\partial z} - \frac{\Delta}{2} \frac{\partial v}{\partial z} \right]_{z=0} \text{ and}$$

$$Cf_y = \left((\mu + K) \frac{\partial v^*}{\partial z^*} + K \omega_2^* \right)_{z^*=0} = \rho U_r^2 \left[(1 + \Delta) \frac{\partial v}{\partial z} + \frac{\Delta}{2} \frac{\partial u}{\partial z} \right]_{z=0}$$

$$Cw_x = \frac{Mw_x v^2}{\gamma U_r^3} = \left(\frac{\partial \omega_1}{\partial z} \right)_{z=0} \text{ where } Mw_x = \gamma \left(\frac{\partial \omega_1^*}{\partial z^*} \right)_{z^*=0} = \frac{\gamma U_r^3}{v^2} \frac{\partial \omega_1}{\partial z};$$

$$Cw_y = \frac{Mw_y v^2}{\gamma U_r^3} = \left(\frac{\partial \omega_2}{\partial z} \right)_{z=0} \text{ where } Mw_y = \gamma \left(\frac{\partial \omega_2^*}{\partial z^*} \right)_{z^*=0} = \frac{\gamma U_r^3}{v^2} \frac{\partial \omega_2}{\partial z}$$

In addition to that rate of heat transfer and rate of mass transfer at the surface of wall are

$$Nu = x \frac{q_w}{k(T_w - T_\infty)} \text{ and } Sh = x \frac{q_m}{D(C_w - C_\infty)} \text{ Where } q_w = - \left[\left(k + \frac{16 \sigma T^3}{3k} \right) \frac{\partial T}{\partial z} \right]_{z^* = 0} ,$$

$$q_m = -D \left[\frac{\partial C}{\partial z} \right]_{z^* = 0}$$

Finally, following skin friction, wall couple stress, Sherwood number and Nusselt number in non-dimensional for are

Skin-friction is obtained as,

$$C_{f_x} = \rho U_r^2 \left[(1+\Delta) \frac{\partial u}{\partial z} - \frac{\Delta}{2} \frac{\partial v}{\partial z} \right], \quad C_{f_y} = \rho U_r^2 \left[(1+\Delta) \frac{\partial v}{\partial z} + \frac{\Delta}{2} \frac{\partial u}{\partial z} \right] \quad (23)$$

Wall couple stress is obtained as,

$$C_{w_x} = \left[\frac{\partial \omega_1}{\partial z} \right]_{z=0}, \quad C_{w_x} = \left[\frac{\partial \omega_2}{\partial z} \right]_{z=0} \quad (24)$$

The plate surface rate of the heat transfer i.e. Nusselt number emerges as

$$\frac{Nu}{\sqrt{Re_x}} = -(1+F) \left[\frac{\partial \theta}{\partial z} \right]_{z=0} \quad (25)$$

The plate surface rate of mass transfer i.e. Sherwood number is calculated with

$$\frac{Sh}{\sqrt{Re_x}} = - \left[\frac{\partial \phi}{\partial z} \right]_{z=0} \quad (26)$$

Where $Re_x = x U_r / \nu$ is Reynolds number.

3 Finite element method numerical solution

The set of partial differential Eqs. (16-21) subject to initial and boundary conditions (22) are nonlinear, coupled and therefore it cannot be solved analytically. The variational form is particularly popular for fluid mechanics simulations and general details of this methodology are available in many textbooks [Reddy (1985); Entwistle (1999)]. Furthermore, explicit applications and details of the Finite element method can be found in Beg et al. [Beg, Rashidi and Bhargava (2011)]. Although the method has been used in many micropolar fluid mechanics problems, most applications have been steady-state. Recent unsteady micropolar flow studies employing FEM (Finite Element Method) include magnetic nanofluid cavity flow and micropolar flow from an oblique surface [Thumma, Beg and Siva Reddy (2017); Shamshuddin, Beg, Ram et al. (2017)]. The basic fundamental steps involved in Finite element method are documented indeatil with complete solution can be refeered in Shamshuddin et al. [Shamshuddin, Beg, Siva Reddy et al. (2017)].

In general, to verify that the converged solutions are indeed correct, i.e. to guarantee grid (mesh) independency, a grid refinement test is carried out by dividing the whole domain into successively sized grids 81×81, 101×101 and 121×121 in the z-axis direction.

Furthermore, the finite element code is run for different grid sizes and for a grid size of 101×101 the solutions are observed to achieve mesh independence. Therefore, for all subsequent computations, a grid size of 101 intervals is elected with $h=0.01$. After element assembly 6 functions are to be evaluated at each node then we get a set of 606 non-linear equations and then using boundary conditions iterative scheme is applied to solve those non-linear equations until the solution is assumed to be convergent i.e. the iterative process is terminated when the following condition is fulfilled:

$\sum_{i,j} |\xi^{n+1} - \xi^n| \leq 10^{-6}$, where $\xi = u, v, \omega_1, \omega_2, \theta, \phi$ and n denotes the iterative step. This criterion maintains high accuracy for coupled multi-physical boundary layer equations. Once the key variables are computed, a number of wall gradient functions may be automatically evaluated.

4 Grid sensitivity and validation of FEM solutions

The numerical values of primary and secondary velocities u, v , primary and secondary angular velocities ω_1, ω_2 , temperature θ and concentration ϕ for different grid sizes are shown in Tab. 1. From this it reflects the physically realistic results. Hence, this method has been proven to be adequate and gives adequate results for conservation equations.

Table 1: Numerical values of $u, v, \omega_1, \omega_2, \theta, \phi$ for variations of mesh sizes

Grid Size=0.01					
u	v	ω_1	ω_2	θ	ϕ
1.015	0	-0.55	0.55	1	1
3.692615	-3.777113	-0.344104	0.344104	0.575667	0.418662
5.645103	-5.549523	-0.189119	0.189120	0.292743	0.175343
4.075523	-4.155844	-0.070451	0.070440	0.149121	0.075861
2.606545	-2.630525	-0.035045	0.035045	0.063523	0.033802
1.531605	-1.534532	-0.024623	0.024623	0.030118	0.015111
0.909117	-0.921104	-0.020441	0.020441	0.012606	0.006854
0.559544	-0.557105	-0.008171	0.008171	0.005211	0.002937
0.252822	-0.251117	-0.005125	0.005135	0.002315	0.001311
0.053531	-0.056608	-0.002644	0.002644	0.000917	0.000310
Grid Size=0.001					
1.015	0	-0.55	0.55	1	1
3.692405	-3.776982	-0.343823	0.343823	0.575532	0.418531
5.644923	-5.549453	-0.188902	0.188902	0.292684	0.175264
4.075389	-4.155689	-0.069839	0.069839	0.148898	0.075683
2.606499	-2.630387	-0.034792	0.034792	0.063384	0.033745
1.531485	-1.534412	-0.024565	0.024565	0.029771	0.015003
0.908921	-0.920543	-0.019892	0.019892	0.012580	0.006678
0.559388	-0.557011	-0.007893	0.007893	0.005115	0.002786
0.252764	-0.251002	-0.005041	0.005041	0.002276	0.001188

0.053411	-0.056522	-0.002580	0.002582	0.000874	0.000286
Grid Size=0.001					
1.015	0	-0.55	0.55	1	1
3.692201	-3.776772	-0.343645	0.343645	0.57539	0.418488
5.643745	-5.549309	-0.188792	0.188792	0.292644	0.175198
4.075221	-4.155566	-0.069691	0.069691	0.148093	0.075481
2.606287	-2.630198	-0.034596	0.034596	0.063222	0.033594
1.531299	-1.534229	-0.024387	0.024384	0.029759	0.014987
0.908765	-0.920388	-0.019665	0.019662	0.012564	0.006586
0.559198	-0.556762	-0.007700	0.007700	0.005000	0.002589
0.252666	-0.250000	-0.005000	0.005000	0.002093	0.001000
0.053299	-0.056379	-0.002559	0.002559	0.000868	0.000286

Table 2: Comparison of C_f and C_w when $F = 0, Ec = 0$ and $\alpha = 0$

				Bakr [Bakr (2011, 2013)] Perturbation Solutions	Present Numerical Solutions			
Δ	Kr	R	S	C_f	C_w	C_f	C_w	
0.2	0.01	0.2	1.0	5.661	1.591	5.660881	1.590083	
0.4	0.01	0.2	1.0	6.078	1.133	6.078016	1.133432	
1.0	0.01	0.2	1.0	7.010	0.631	7.010023	0.631119	
0.2	0.5	0.2	1.0	5.634	1.153	5.634002	1.152577	
0.2	1.0	0.2	1.0	4.841	0.990	4.842012	0.990091	
0.2	0.01	0.4	1.0	3.917	1.274	3.917431	1.273590	
0.2	0.01	0.6	1.0	2.607	0.889	2.607218	0.890221	
0.2	0.01	0.2	1.5	6.564	3.346	6.564401	3.346333	
0.2	0.01	0.2	2.0	6.552	6.533	6.551669	6.533228	

Table 3: Comparison of Cf_x, Cf_y, Cw_x, Cw_y for Q, Gr, Gm when $F = 0, Ec = 0, Kr = 0$ and $\alpha = 0$

			Bakr [Bakr (2011, 2013)] Perturbation Solutions				Present Numerical Solutions			
Q	Gr	Gm	Cf_x	Cf_y	Cw_x	Cw_y	Cf_x	Cf_y	Cw_x	Cw_y
0.5	10	4.0	2.3	-0.11	-	-	2.372	-	-	-
			73		0.015	0.08	902	0.108910	0.014881	0.080013
1.0	10	4.0	2.8	-	-	-0.9	2.8200	-	-	-0.9467
			19	0.123	0.017	47	13	0.123115	0.017101	91
0.5	5.0	4.0	0.881	0.078	-0.0	-0.6	0.8809	0.077890	-0.0190	-0.6046
			19		05	01		16	10	
0.5	10	2.0	1.7	0.3	-0.0	-0.7	1.798817	0.3227	-0.0200	-0.7060
			99	23	20	06		01	11	13

Tab. 2 presents a comparison between analytical and numerical results for Δ, Kr, R and S . It must be mentioned that in the case of $F = 0, Ec = 0$ and $\alpha = 0$ the present results are

excellent agreement with those reported results [Bakr (2011)] for some limiting case. Tabs. 3 and 4 depicts the comparison between analytical and numerical results for various parameters on Cf_x, Cf_y, Cw_x, Cw_y for the case of $F=0, Ec=0, Kr=0$ and $\alpha=0$, the present results are excellent agreement with the results reported by Bakr [Bakr (2013)]. Furthermore, CPU took 6.52 seconds to compute the velocities and angular velocities profiles, 5.37 seconds to compute the temperature profiles, 4.96 seconds to compute the concentration profiles for 1001 nodal points with the Intel CORE i3 processor under windows platform, which are computed by using the Matlab command tic; {statements} toc;

Table 4: Comparison of Cf_x, Cf_y, Cw_x, Cw_y for M, K, Pr, Sc when $F=0, Ec=0, Kr=0$ and $\alpha=0$

M	K	Pr	Sc	Bakr [Bakr (2011, 2013)] Perturbation Solutions				Present Numerical Solutions			
				Cf_x	Cf_y	Cw_x	Cw_y	Cf_x	Cf_y	Cw_x	Cw_y
0.5	0.5	0.7	0.6	7.716	2.548	-0.047	-1.344	7.715 994	2.5482 10	-0.047012	-1.344231
1.0	0.5	0.7	0.6	6.846	2.086	-0.039	-1.249	6.846 032	2.0857 09	-0.039034	-1.248871
2.0	0.5	0.7	0.6	5.490	1.490	-0.031	-1.102	5.486 109	1.4900 52	-0.030947	-1.102212
0.5	1.0	0.7	0.6	10.25	4.421	-0.079	-1.623	10.25 0023	4.4223 01	-0.079231	-1.622651
0.5	2.0	0.7	0.6	12.58	6.95	-0.123	-1.856	12.57 6051	6.9503 33	-0.123111	-1.857010
0.5	0.5	1.0	0.6	7.457	2.427	-0.045	-1.315	7.457 341	2.4269 78	-0.045063	-1.315230
0.5	0.5	3.0	0.6	5.939	1.751	-0.037	-1.146	5.941 220	1.7511 32	-0.036690	-1.146220
2.0	0.5	0.7	1.0	5.302	1.424	-0.03	-1.081	5.301 765	1.4244 41	-0.030036	-1.081003

5 Results and discussions

A numerical approach is used for reduced governing equations into a nonlinear partial differential equation using dimensionless quantities with associate initial and boundary conditions. Eqs. (16-21) subject to initial and boundary conditions (22) has been solved with a robust finite element method, weighted residual approach for emerging physical parameters. The evolution of translation velocity components (u, v), microrotation velocity components (ω_1, ω_2), temperature (θ) and concentration (ϕ) profiles are illustrated in Figs. 2-23, for selected parameters i.e. Δ, S, R, F, Q , and Kr . The following default parameter values are implemented in all the finite element computation $nt = \pi / 2, \epsilon = 0.01, n = 10, Gr = 10, Gm = 4, M = 0.5, K = 5, Sc = 0.6, Pr = 0.7, \Delta = 0.2, \alpha = \pi / 4, S = 1, R = 0.2, F = 0.5, Q = 1, Ec = 0.01, Kr = 0.5$.

All graphs therefore correspond to these values unless specifically indicated otherwise. Weak transverse magnetic field ($M=0.5$) and strong thermal and species buoyancy effects

are considered. High permeability is examined (when $K \rightarrow \infty$ the purely fluid regime is recovered i.e. vanishing porous media fibers, and the Darcian drag components in the primary and secondary momenta equation $-(1/K)u$ and $-(1/K)v$ vanish.

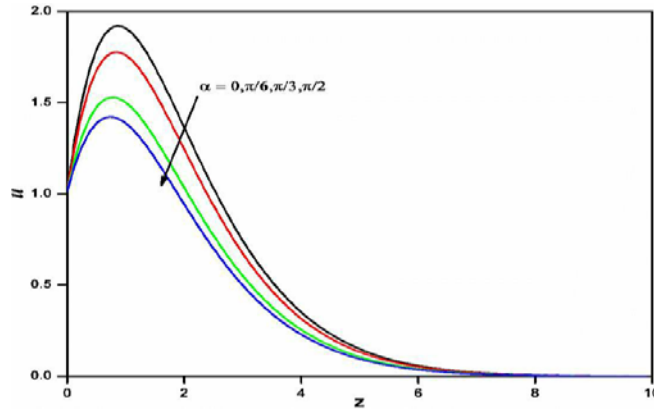


Figure 2: Effect of α on velocity profiles

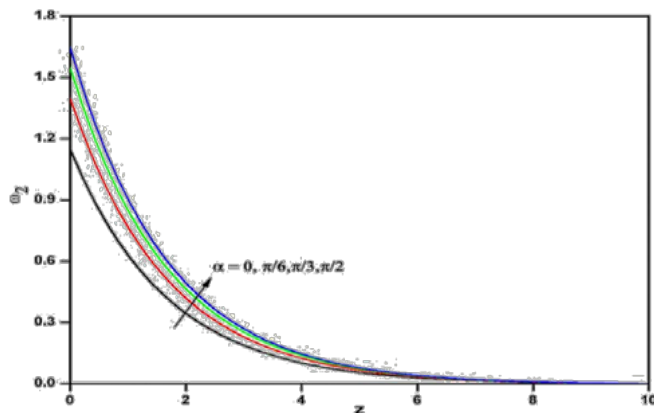


Figure 3: Effect of α on angular velocity profiles

Figs. 2-3 show the pattern of translational velocity and angular velocity profiles for angle of inclination. It is clearly observed that velocity is decreased with an increase of angle of inclination. This is attributable to the greater drag experienced at the plate surface relative to the decrease in thermal and species buoyancy forces. Greater effort is therefore needed to drive the micropolar fluid along the plate. Furthermore, the buoyancy effects decrease to a component of the maximum buoyancy force for a vertical plate, since the buoyancy forces scale with the factor $\cos \alpha$. Hence the fluid attains high velocity profiles for the vertical plate, $\alpha=0$ and progressively decreases with greater inclination of the plate, while the opposite behavior is observed for micro-rotation i.e. angular velocity. The plate inclination induces a significant modification in both linear and angular velocity distributions because with greater plate inclination, there is a deceleration in the linear flow and acceleration in the angular flow.

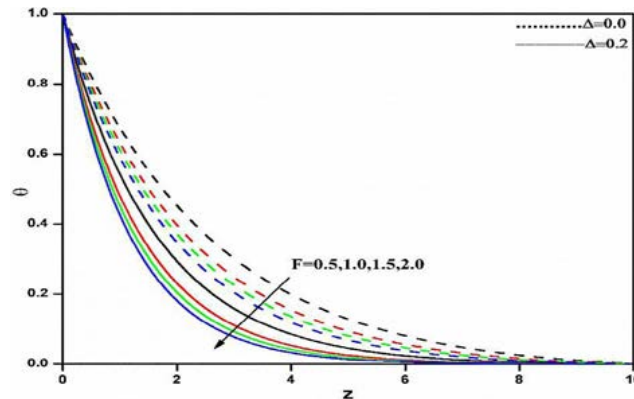


Figure 4: Effect of F on temperature profiles

The variations of the temperature profiles for different values of thermal radiation parameter F for both Newtonian and polar fluid are presented in Fig. 4. The thermal radiation parameter features in the augmented thermal diffusion term in the Eq. (21), since the thermal conduction is dominant for large values of F , therefore as F increases the temperature of the surface decreases and reduces the thermal boundary layer thickness. Further, it is also observed that fluid temperature is lower for polar fluids than for Newtonian fluids.

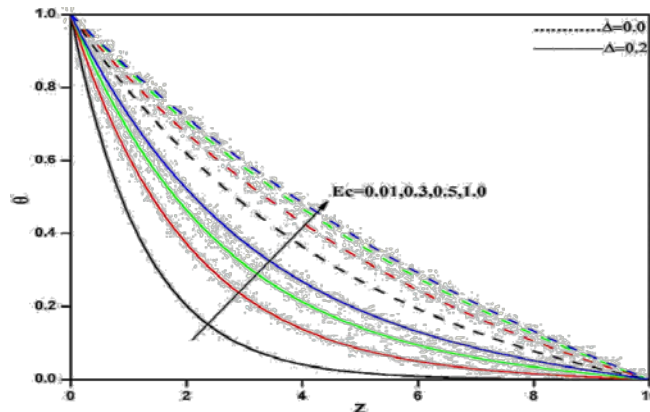


Figure 5: Effect of Ec on temperature profiles

Fig. 5 presents the effect of Eckert number on temperature profiles. Ec expresses the relative contribution of kinetic energy in the flow and the enthalpy difference in the boundary layer. It personifies the conversion of kinetic energy into thermal energy by work done against the viscous fluid stresses. It is a significant parameter in low speed non-Newtonian flows wherein dissipation effects are not trivial etc. Positive Eckert number implies cooling of the wall and therefore a transfer of heat to the micropolar fluid. Free convection is enhanced and we observe in consistency with this temperature is markedly boosted. Thermal boundary layer thickness is also therefore increased with greater Eckert number.

Variations of viscosity ratio parameter Δ on u, v distributions (Fig. 6) is significantly enhanced with transverse coordinate (normal to the plate) with maximum acceleration computed a short distance from the plate surface. No cross-over of profiles is observed and positive magnitudes are sustained indicating that backflow never arises. In addition, the angular velocity (Microrotation) distribution profiles are presented in the Fig. 7, which present consistent variations with an increment of Δ i.e. ω_1 decreases and ω_2 increases, which occurs due to the presence of increasing concentration of micro-elements which enhances vortex viscosity therefore also damps the gyratory motions of micro-elements. The maximum influence is at the wall since with greater concentration of micro-elements, these micro-elements are physically impaired from rotating near the boundary more than anywhere else in the fluid regime. This effect is progressively reduced with distance from the plate.

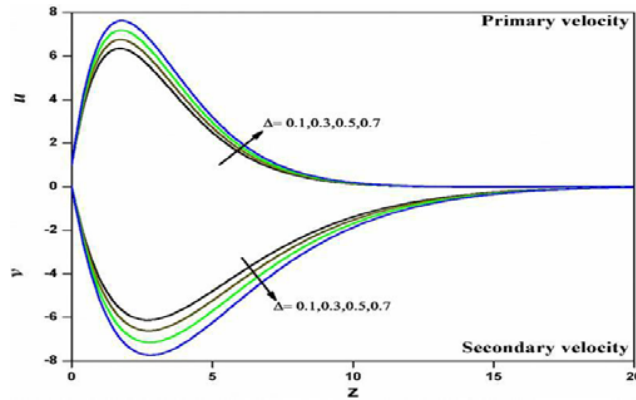


Figure 6: Effect of Δ on primary and secondary velocity profiles

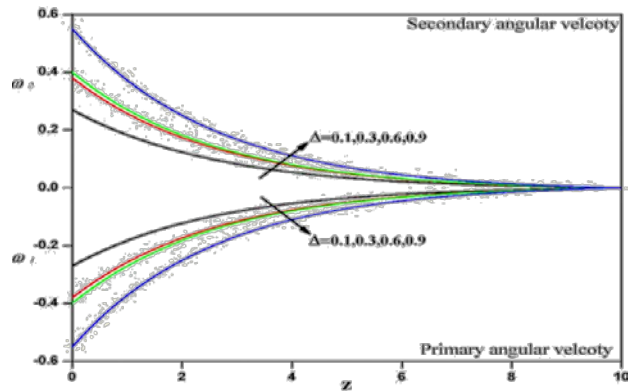


Figure 7: Effect of Δ on primary and secondary angular velocity profiles

The translational velocity and the angular velocity profiles for different values of Grashof number Gr and modified Grashof number Gm are illustrated respectively in Figs. 8-9. It is noticed that the translational velocity increases as Gr or Gm increases. Furthermore, the peak value of velocity increases rapidly near the wall of the porous plate. However,

the similar behavior is quantified in the case of angular velocity profiles. The positive values of Gr corresponds to cooling of the surface by natural convection.

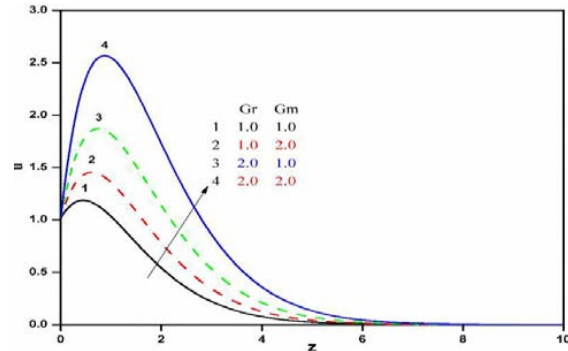


Figure 8: Effect of Gr & Gm on velocity profiles

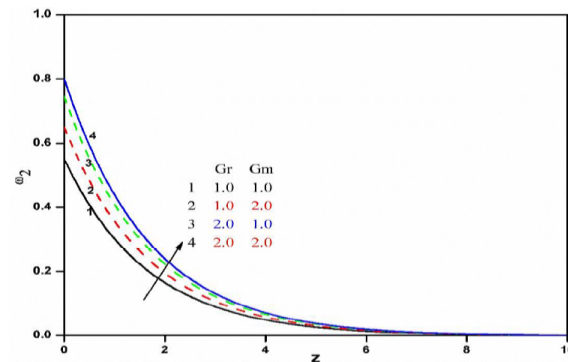


Figure 9: Effect of Gr & Gm on Angular velocity profiles

Fig. 10 shows the pattern of the primary as well as secondary velocities for different values of magnetic field parameter. It is noticed that primary velocity u decreases whereas secondary velocity v increases which indicates that the magnetic field tends to accelerate primary flow whereas reverse effect on secondary due to imposition of transverse magnetic field of strength B_0 generates in the electrically-conducting micropolar fluid a resistive type of force, called Lorentz force, which acts against the relative motion of the fluid.

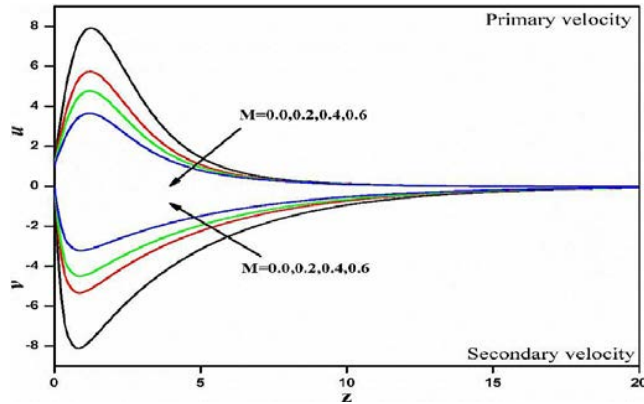


Figure 10: Effect of M on primary and secondary velocity profiles

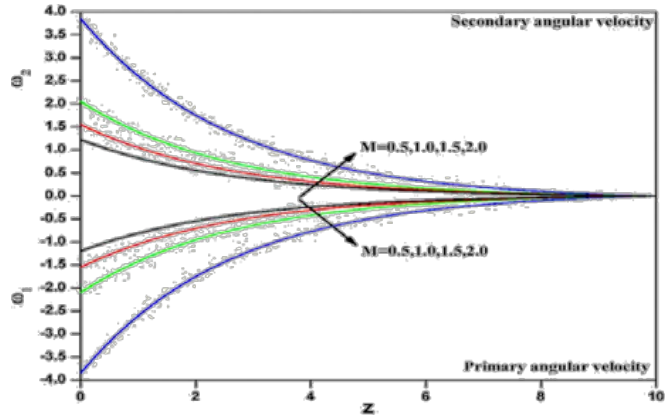


Figure 11: Effect of M on primary and secondary angular velocity profiles

Similarly, in Fig. 11 an increase in magnetic field parameter is observed to significantly decelerate the primary angular velocity i.e. reduce the magnitude of microrotation, although the effect is more localized at the plate surface and progressively decays further from the plate. The primary angular velocity field is influenced indirectly via the deceleration in the linear velocity via the coupling term $+\Delta(\partial\omega_1 / \partial z)$. While the secondary angular velocity significantly accelerates since the term $-\Delta(\partial\omega_2 / \partial z)$ couples the secondary angular velocity field.

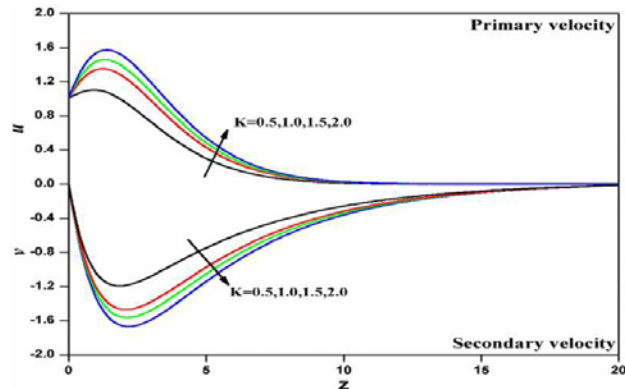


Figure 12: Effect of K on primary and secondary velocity profiles

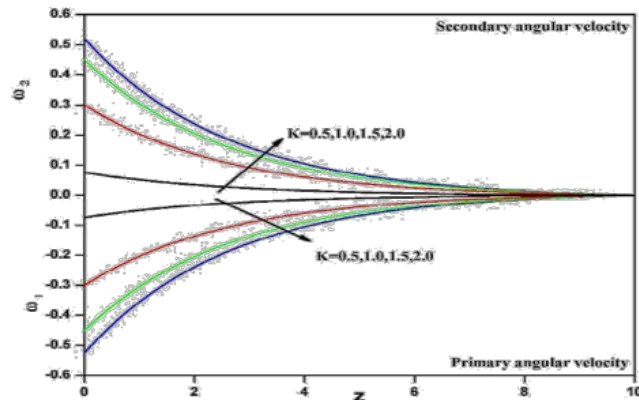


Figure 13: Effect of K on primary and secondary angular velocity profiles

Variations of the permeability parameter (K) on both u, v distributions (Fig. 12) are visualized graphically. This parameter characterizes the hydraulic transmissivity of the porous medium. It arises in the Darcian drag force term in the composite linear momentum Eqs. (11) and (12), viz $-(1/K)u$ and $-(1/K)v$. As permeability increases the regime solid fibers progressively decrease. This results in an acceleration in primary velocity and deceleration in secondary velocity. The implication for MHD energy generators is that the flow can be damped strategically via the introduction of a porous material in the flow zone and accelerated with higher permeability media. Similarly, the primary angular velocity is reduced and secondary velocity enhances with greater permeability parameter as shown in Fig. 13. The increase in permeability implies greater void space in the porous medium. This allows an enhancement in gyratory motions as the micro-elements are afforded greater space in which to spin.

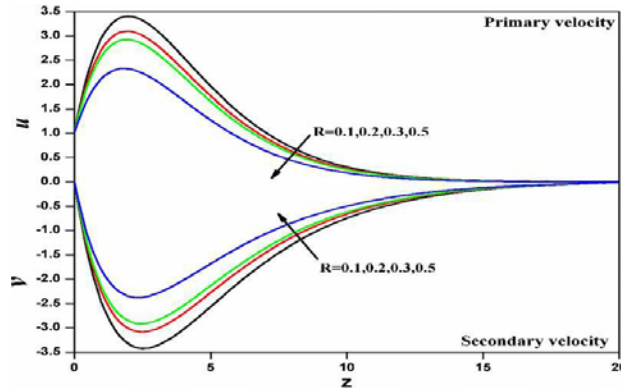


Figure 14: Effect of R on primary and secondary velocity profiles

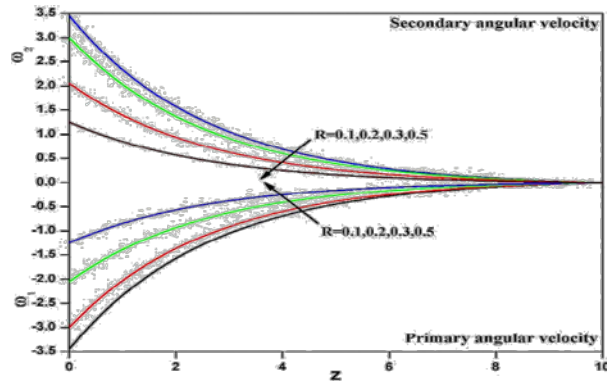


Figure 15: Effect of R on primary and secondary angular velocity profiles

Variations of rotation parameter R versus u, v and ω_1, ω_2 profiles were studied in Figs. 14-15. The results show that primary velocity decreases as rotation parameter R decreases and conversely enhances the secondary velocity. A reverse phenomenon is observed in primary and secondary angular velocities i.e. primary angular velocity increases and secondary angular velocity decreases as R increases. The rotational parameter, R , features in the so-called “cross flow terms”. As R increases the centrifugal force increases (faster angular velocity of rotation of the plate, Ω). The centrifugal effect influences each velocity field via the rotational body force term in the other velocity field equation. Although both terms are negative, only primary linear flow is decelerated and the compensation in momentum assists the secondary flow field. The micropolar coupling terms in both linear momenta equations i.e. $(1+\Delta)(\partial^2 u / \partial z^2)$, $(1+\Delta)(\partial^2 v / \partial z^2)$ and additionally the angular momentum coupling terms, viz. $-\Delta(\partial \omega_2 / \partial z)$ and $+\Delta(\partial \omega_1 / \partial z)$, enable the rotational body force effect to impart a considerable influence on the micro-rotation field components. The primary spin of micro-elements is effectively accelerated whereas the secondary spin is retarded. Gyration is therefore substantially modified by rotational (centrifugal) body force.

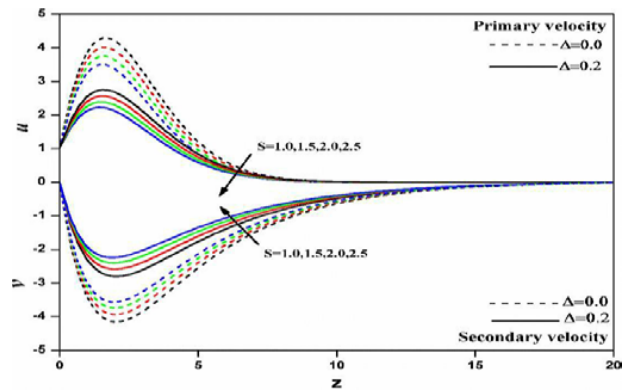


Figure 16: Effect of S on primary and secondary velocity profiles

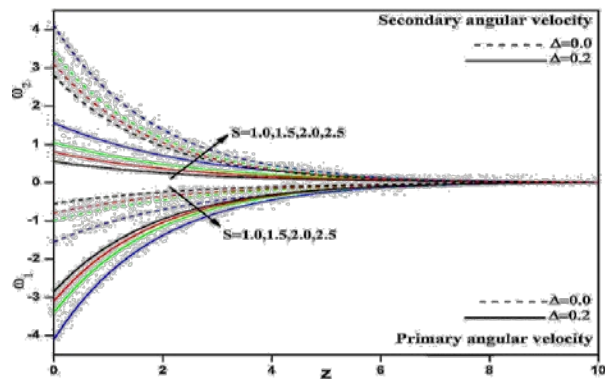


Figure 17: Effect of S on primary and secondary angular velocity profiles

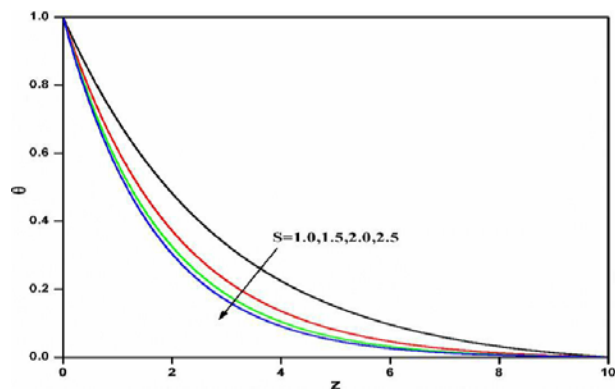


Figure 18: Effect of S on temperature profiles

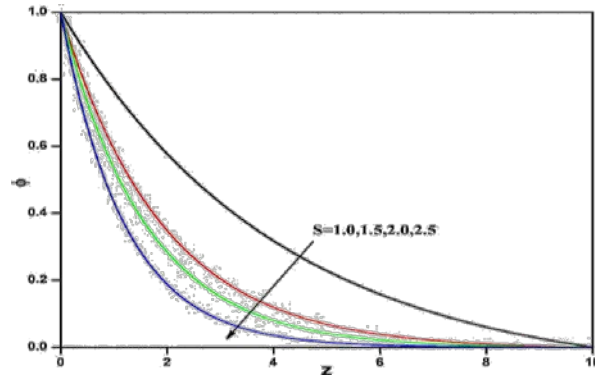


Figure 19: Effect of S on concentration profiles

Figs. 16-19 present the response in u, v and ω_1, ω_2 profiles for various values of suction parameter S against spanwise coordinate, z . Fig. 16 shows that increasing suction significantly decreases u i.e. decelerates the boundary layer flow. Greater suction corresponds physically to removal of micropolar fluid via the wall. This destroys momentum, and causes the boundary layer to adhere to the wall thereby stabilizing boundary layer growth due to which the primary velocity of the fluid decreases. But, secondary velocity accelerates the flow. Since the case $S < 0$ corresponds to blowing (mass injection) at the wall and is not relevant to the current study and has therefore not been addressed. A similar behavior is observed in case of ω_1, ω_2 i.e. ω_1 decreases because primary angular momentum field (micro-rotation) retards gyratory motion (spin) of micro-elements which leads to a decrease and ω_2 accelerates gyratory motion (spin) of micro-elements which leads to increase. Further, it is also observed that fluid velocity and angular velocity is lower for polar fluids than for Newtonian fluids (as depicted in Fig. 17). The temperature and concentrations profiles for are presented in Figs. 18-19, from these figures it is revealed that the presence of suction parameter S diminishes the both temperature and concentration distribution. Hence the profiles attain their maximum value at the wall and decrease exponentially with z and finally tend to zero as $z \rightarrow \infty$. Further it is found to be good agreement with boundary conditions given in Eq. (17).

The variations of the temperature profiles for different values of Prandtl number Pr is presented in Fig. 20. The temperature decays quickly for large values of Prandtl number, the reason underlying such a behavior is that the smaller values of Pr are equivalent to increasing thermal conductivities, and therefore heat is able to diffuse away from the heated plate more rapidly than for higher values of Pr . Hence in the case of smaller Pr as the boundary layer thicker and rate of heat transfer is reduced. Some similar variations also observed for the temperature profiles of heat absorption parameter Q , fluid temperature reduces due to tendency of heat absorption. Greater heat absorption Q clearly reduces the temperatures in the domain as observed in Fig. 21, and the effect is most prominent at the wall (plate surface).

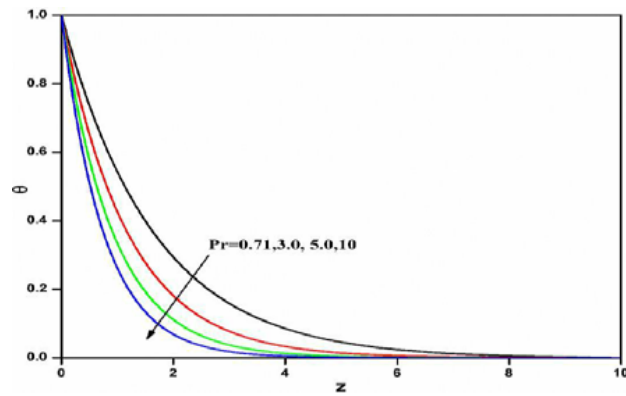


Figure 20: Effect of Pr on temperature profiles

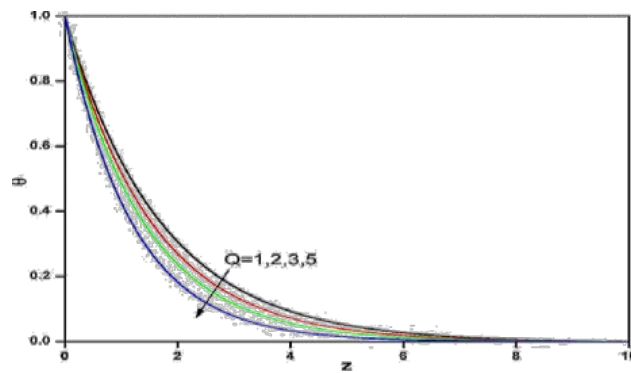


Figure 21: Effect of Q on temperature profiles

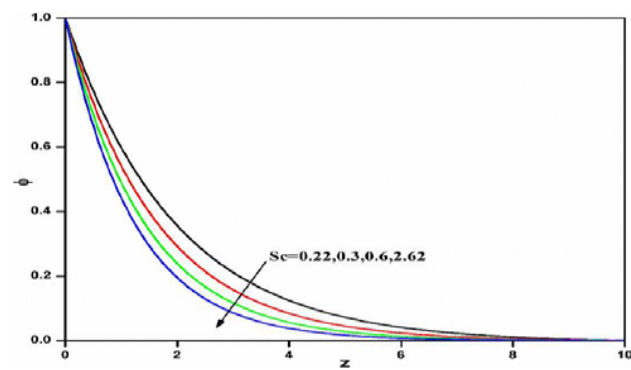


Figure 22: Effect of Sc on concentration profiles

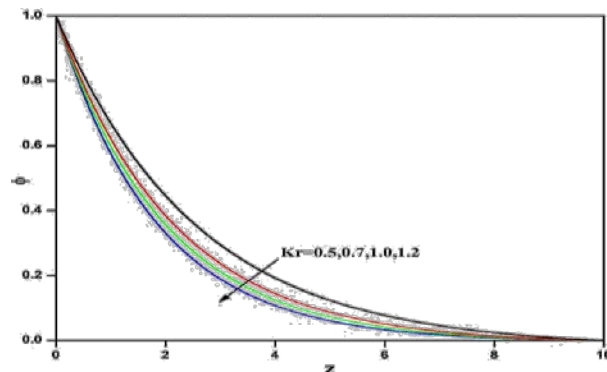


Figure 23: Effect of Kr on concentration profiles

Figs. 22-23 show concentration profiles for different values of Schmidt number Sc and chemical reaction parameter Kr . The values of Sc are chosen as $Sc = 0.22$ (hydrogen), $Sc = 0.3$ (helium), $Sc = 0.6$ (water vapour) and $Sc = 2.62$ (propyl benzene) at 25°C temperature and one atmospheric pressure. It is inferred that concentration profiles decrease at all the points in the flow field with increase of Sc , because smaller values of Sc are equivalent to increasing chemical molecular diffusivity. Hence mass diffusion tends to enhance species concentration. A similar trend is also seen in case of chemical reaction parameter Kr , due to consumption of chemical, the concentration profiles decreases rapidly as Kr increases, which represents that effect of chemical reaction is prominent due to changes in diffusion rates.

6 Conclusions

In present paper, a numerical investigation has been carried out to obtain solutions for unsteady MHD free convective micropolar fluid through an inclined rotating oscillating porous plate with thermal radiation and dissipation effects. The time dependent conservation equations for momentum, angular momentum (micro-rotation component), energy and concentration have been non-dimensionalized with appropriate variables. The resulting non-linear, transient, coupled system of partial differential equations and set of initial and boundary conditions has been solved using the variational finite element method with a Galerkin weighted residual scheme. We investigated an interesting primary as well secondary translation velocities and angular velocities, temperature and concentration profiles for various pertinent parameters which came into the flow are discussed in detail. The important findings are summarized as below:

- Primary linear flow for viscosity ratio parameter, Permeability parameter, Grashof and modified Grashof number tend to enhance the momentum boundary layer but reverse effect is observed for magnetic field parameter, wall suction parameter and rotation (centrifugal) parameter.
- Secondary linear flow for viscosity ratio parameter, magnetic field parameter, wall suction parameter and rotation parameter tend to enhance the momentum boundary layer but reverse effect is observed for permeability parameter.

- Primary angular velocity increases as R tend to enhance, but reverse phenomenon is noticed for Δ , M , K and S . Similarly in case of secondary angular velocity increases as Δ , M , K and S increases, but decreases as R increases.
- Angular velocity (micro-rotation) is suppressed and micro-rotation boundary layer thickness increased with increasing angle of inclination (α).
- The flow is accelerated and momentum boundary layer thickness decreased with increasing values Gr , Gm but inclination parameter shows reverse effect. But, in case of microrotation all Gr , Gm , and α increases.
- The temperature of the micropolar fluid and thermal boundary layer thickness are both decreased with increasing of F , S , Pr and Q . But the temperature of the fluid increases with an increase of Eckert number.
- Reactive solute concentration and concentration boundary layer thickness is suppressed with increasing wall suction, Schmidt number and first order chemical reaction parameter.
- The present numerical results are found to be in excellent agreement with the published results.

Reference

- Abdelkhalek, M. M.** (2008): Radiation and dissipation effect on unsteady MHD micropolar flow past an infinite vertical plate in porous medium with time dependent suction. *Indian Journal of Physics*, vol. 82, no. 4, pp. 415-434.
- Anika, N. N.; Hoque, M. M.** (2013): Thermal buoyancy force effects on developed flow considering hall and ion-slip current. *Annals of Pure and Applied Mathematics*, vol. 3, no. 2, pp. 179-188.
- Anika, N. N.; Hoque, M. M.; Hossain, S. I.; Alam, M. M.** (2015): Thermal diffusion effect on unsteady viscous MHD micropolar fluid flow through an infinite plate with hall and Ion-slip current. *Procedia Engineering*, vol. 105, pp. 160-166.
- Anika, N. N.; Hoque, M. M.; Islam, N.** (2013): Hall current effects on Magnetohydrodynamics fluid over an infinite rotating vertical porous plate embedded in unsteady laminar flow. *Annals of Pure and Applied Mathematics*, vol. 3, no. 2, pp. 189-200.
- Arifuzzaman, S. M.; Rana, B. M. J.; Ahmed, R.; Ahmmed, S. F.** (2017): Cross diffusion and MHD effect on a higher order chemically reactive micropolar fluid of naturally convective heat and mass transfer past through an infinite vertical porous medium with a constant heat sink. *AIP Conference Proceedings*.
- Ariman, T.; Turk, M. A.; Sylvester, N. D.** (1973): Applications of micro continuum fluid mechanics: a review. *International Journal of Engineering Science*, vol. 11, pp. 905-930.
- Ariman, T.; Turk, M. A.; Sylvester, N. D.** (1974): Applications of micro continuum fluid mechanics: a review. *International Journal of Engineering Science*, vol. 12, pp. 273-293.
- Baag, S.; Mishra, S. R.; Hoque, M. M.** (2018): Magnetohydrodynamics boundary layer flow over an exponentially stretching sheet past a porous medium with uniform heat source. *Journal of Nanofluids*, vol. 7, no. 3, pp. 570-576.

- Babu, D. H.; Satya Narayana, P. V.** (2016): Joule heating effects on MHD mixed convection of a Jeffery fluid over a stretching sheet with power law heat flux: a numerical study. *Journal of Magnetism and Magnetic Materials*, vol. 412, pp. 185-193.
- Bakr, A. A.** (2011): Effect of chemical reaction on MHD free convection and mass transfer flow of a micropolar fluid with oscillatory plate velocity and constant heat source in a rotating frame of reference. *Communication in Nonlinear Science and Numerical Simulation*, vol. 16, pp. 698-719.
- Bakr, A. A.** (2013): Combined heat and mass transfer in magneto-micropolar fluid flow with thermal radiation in a rotating frame of reference. *International Journal of Energy & Technology*, vol. 5, no. 10, pp. 1-9.
- Bakr, A. A.; Chamkha, A. J.** (2017): Oscillatory free convection of a micropolar rotating fluid on a vertical plate with variable heat flux and thermal radiation. *Heat Transfer Research*, vol. 48, no. 2, pp. 139-159.
- Batchelor, G. K.** (1967): *An introduction to fluid dynamics*. Cambridge University Press, UK.
- Beg, O. A.; Ghosh, S. K.; Narahari, M.** (2010): Mathematical modelling of oscillatory MHD Couette flow in a rotating highly permeable medium permeated by an oblique magnetic field. *Chemical Engineering and Communication*, vol. 198, pp. 235-254.
- Bég, O. A.; Rashidi, M. M.; Bhargava, R.** (2011): *Numerical simulation in micropolar fluid dynamics*. Lambert: Sarbrücken, Germany.
- Brewster, M. Q.** (1992): *Thermal radiative transfer and properties*. John Wiley, New York.
- Chaudhary, R. C.; Preeti, J.** (2014): Influence of hall current on chemically reacting micropolar fluid flow from radiative rotating surface with variable suction and Soret effect in slip flow regime. *Journal of Rajasthan Academy Physical Sciences*, vol. 13, no. 3-4, pp. 317-348.
- Cortell, R.** (2008): A numerical tackling on Sakiadis flow with thermal radiation. *Chinese Physics Letters*, vol. 25, pp. 1340-1342.
- Cowling, T. G.** (1957): *Magnetohydrodynamics*. Wiley inter science, Newyork.
- Das, K.** (2011): Effect of chemical reaction and thermal radiation on heat and mass transfer flow of micropolar fluid in a rotating frame of reference. *International Journal of Heat Mass Transfer*, vol. 54, pp. 3505-3513.
- Entwistle, K. M.** (1999): *Basic principles of the finite element method*. Institute of materials, London.
- Eringen, A. C.** (1966): A unified theory of thermomechanical material. *International Journal of Engineering Science*, vol. 4, no. 2, pp. 179-202.
- Ganapathy, R. A.** (1994): A note on oscillatory coquette flow in a rotating system. *ASME Journal of Applied Mechanics*, vol. 61, pp. 208-209.
- Gibanov, N. S.; Sheremet, M. A.; Pop, I.** (2016): Natural convection of micropolar fluid in wavy differentially heated cavity. *Journal of Molecular Liquids*, vol. 221, pp. 518-525.
- Gosh, S. K.; Beg, O. A.; Narahari, M.** (2007): Hall effects on MHD flow in a rotating system with heat transfer characteristics. *Meccanica*, vol. 42, no. 3, pp. 247-262.

Hayat, T.; Farooq, S.; Ahmad, B.; Alsaedi, A. (2016): Homogeneous-heterogeneous reaction and heat source/sink effects in MHD Peristaltic flow of micropolar fluid with Newtonian heating in a curved channel. *Journal of Molecular Liquids*, vol. 223, pp. 469-488.

Hayat, T.; Sajjad, R.; Ellahi, R.; Alsaedi, A.; Muhammad, T. (2017): Homogeneous-heterogeneous reaction in MHD flow of micropolar fluid by a curved stretching surface. *Journal of Molecular Liquids*, vol. 240, pp. 209-220.

Hussain, S. M.; Jain, J.; Seth, G. S.; Rashidi, M. M. (2017): Free convective heat transfer with hall effects, heat absorption and chemical reaction over an accelerated moving plate in rotating system. *Journal of Magnetism and Magnetic Materials*, vol. 422, pp. 112-123.

Iynger, T. K. V.; Geeta Vani, V. (2004): Oscillatory flow of a micropolar fluid generated by the rotary oscillations of two concentric spheres. *International Journal of Engineering Science*, vol. 42, pp. 1035-1059.

Kendoush, A. A. (2013): Similarity solution for heat convection from a porous rotating disk in a flow field. *ASME Journal of Heat Transfer*, vol. 135, pp. 1885-1886.

Khonsari, M. M.; Brewe, D. E. (1994): Effect of viscous dissipation on the lubricant characteristics of micropolar fluids. *Acta Meccanica*, vol. 105, no. 1, pp. 57-68.

Kundu, P. K.; Das, K.; Jana, S. (2015): MHD micropolar fluid flow with thermal radiation and thermal diffusion in a rotating frame. *Bulletin of Malaysian Mathematical Sciences and Society*, vol. 38, pp. 1185-1205.

Lukaszewicz, G. (1999): *Micropolar fluids, Modelling and Simulation*. Birkhauser Boston, Boston.

Maqbool, K.; Ayesha, S.; Idreesa, S.; Beg, O. A. (2016): Analytical solution for magnetohydrodynamic oscillatory rotating plate and channel flows in porous media using a fractional Burgers viscoelastic model. *European Physical Journal Plus*, vol. 131, pp. 140-157.

Mbeledogu, I. U.; Ogulu, A. (2007): Heat and mass transfer of an unsteady MHD natural convection flow of a rotating fluid past a vertical porous flat plate in the presence of radiative heat transfer. *International Journal of Heat and Mass Transfer*, vol. 50, no. 9, pp. 1902-1908.

Miroshnichenko, I. V.; Sheremet, M. A.; Pop, I. (2017): Natural convection in a tepezoidal cavity filled with a micropolar fluid under the effect of a local heat source. *International Journal of Mechanical Sciences*, vol. 120, pp. 182-189.

Modather, M.; Rashad, A. M.; Chamkha, A. J. (2009): An analytical study of MHD heat and mass transfer oscillatory flow of a micropolar fluid over a vertical permeable plate in porous medium. *Turkish Journal of Engineering and Environmental Science*, vol. 33, pp. 245-257.

Modest, M. F. (1992): *Radiation Heat Transfer*. McGraw-Hill, New York.

Nazir, A.; Hussain, S.; Shafique, M. (2015): The rotationally symmetric flow of micropolar fluids in the presence of an infinite rotating disk. *Applied Mathematics*, vol. 6, pp. 430-439.

Olajuwon, B. I.; Oahimire, J. I. (2013): Unsteady free convection heat and mass transfer in an MHD micropolar fluid in the presence of thermo diffusion and thermal radiation. *International Journal of Pure and Applied Mathematics*, vol. 84, pp. 015-037.

Pal, D.; Mondal, G. (2017): Thermal radiation and MHD effects on boundary layer flow of micropolar nanofluid past a stretching sheet with non-uniform heat source/sink. *International Journal of Mechanical Sciences*, vol. 126, pp. 308-318.

Pal, D.; Talukdar, B. (2012): Perturbation technique for unsteady MHD mixed convection periodic flow, heat and mass transfer in micropolar fluid with chemical reaction in the presence of thermal radiation. *Central European Journal of Physics*, vol. 10, pp. 1150-1167.

Raju, C. S. K.; Hoque, M. M.; Anika, N. N.; Mamatha, S.U.; Sharma, P. (2017): Natural convective heat transfer analysis of MHD unsteady Carreau nanofluid over a cone packed with alloy nanoparticles. *Powder Technology*, vol. 317, pp. 408-416.

Raju, C. S. K.; Hoque, M. M.; Sivasankar, T. (2016): Radiative flow of Casson fluid over a moving wedge filled with gyrotactic microorganisms. *Advanced Powder Technology*, vol. 28, pp. 575-583.

Raza, J.; Azizah, M. R.; Omar, Z. (2016): Rheology of micropolar fluid in a channel with changing walls: investigation of multiple solutions. *Journal of Molecular Liquids*, vol. 223, pp. 890-902.

Reddy, M. G. (2015): Thermal radiation and chemical reaction effects on steady convective slip flow with uniform heat and mass flux in the presence of ohmic heating and a heat source. *Fluid Dynamics & Material Processing*, vol. 10, no. 4, pp. 417-442.

Reddy, G. J.; Reddy, K. B.; Kumar, M.; Hoque, M. M. (2018): A molecular dynamic on transient non-Newtonian MHD casson fluid flow dispersion over a radiative vertical cylinder with entropy heat generation. *Journal of Molecular Liquids*, vol. 252, pp. 245-262.

Reddy, J. N. (1985): *An introduction to finite element method*. Mc Graw- Hill, New York.

Rehman, F.; Imran Khan, M.; Sadiq, M.; Malook, A. (2017): MHD flow of carbon in micropolar nanofluid with convective heat transfer in rotating frame. *Journal of Molecular Liquids*, vol. 231, pp. 353-363.

Satya Narayana, P. V.; Venkateswarlu, B.; Venkataramana, S. (2013): Effect of hall current and radiation absorption on MHD micropolar fluid in a rotating system. *Ain Shams Engineering Journal*, vol. 4, pp. 843-854.

Seth, G. S.; Ansari, Md.; Nandkeolyar, R. (2011): MHD natural convection flow with radiative heat transfer past an impulsively moving plate with ramped temperature. *Heat and Mass Transfer*, vol. 47, no. 5, pp. 551-556.

Seth, G. S.; Nandkeolyar, R.; Ansari, S. M. (2013): Effects of thermal radiation and rotation on unsteady hydromagnetic free convection flow past an impulsively moving vertical plate with ramped temperature in porous medium. *Journal of Applied Fluid Mechanics*, vol. 6, no. 1, pp. 27-38.

Seth, G. S.; Sarkar, S. (2015): MHD natural convection heat and mass transfer flow past a time dependent moving vertical plate with ramped temperature in rotating medium with Hall effects, radiation and chemical reaction. *Journal of Mechanics*, vol. 31, pp. 91-104.

Seth, G. S.; Sarkar, S.; Hussian, S. M. (2014): Effects of hall current, radiation and rotation on natural convection heat transfer past a moving plate. *Ain Shams Engineering Journal*, vol. 5, pp. 489-503.

Seth, G. S.; Singh, J. K. (2013): Effect of hall current on unsteady MHD couette flow of class-II in a rotating system. *Journal of Applied Fluid Mechanics*, vol. 6, no. 4, pp. 473-484.

Shamshuddin, M. D.; Beg, O. A.; Ram, M. S.; Kadir, A. (2017): Finite element computation of multi-physical micropolar transport phenomena from an inclined moving plate in porous media. *Indian Journal of Physics*, vol. 92, no. 2, pp. 215-230.

Shamshuddin, M. D.; Beg, O. A.; Siva Reddy, S.; Kadir, A. (2017): Rotating unsteady multi-physico-chemical magneto micropolar transport in porous media. *Computational Thermal Sciences*, (In Press).

Shamshuddin, M. D.; Thumma, T. (2017): Soret and dufour effects on unsteady MHD free convective flow of micropolar fluid with oscillatory plate velocity considering viscous dissipation effects. *Jurnal Teknologi*, vol. 79, no. 4, pp. 123-136.

Sheikholeslami, M.; Hatami, M.; Ganji, D. D. (2014): Micropolar fluid flow and heat transfer in permeable channel using analytical method. *Journal of Molecular Liquids*, vol. 194, pp. 30-36.

Siva Reddy, S.; Shamshuddin, M. D. (2015): Heat and mass transfer on the MHD flow of a micropolar fluid in the presence of viscous dissipation and chemical reaction. *ICCHMT, Procedia Engineering*, vol. 127, pp. 885-892.

Siva Reddy, S.; Shamshuddin, M. D. (2016): Diffusion-thermo and chemical reaction effects on an unsteady MHD free convection flow in a micropolar fluid. *Theoretical and Applied Mechanics*, vol. 43, pp. 117-131.

Tetbirt, A.; Bouaziz, M. N.; Tahar Abbes, M. (2016): Numerical study of magnetic effect on the velocity distribution field in a macro/micro-scale of micropolar and viscous fluid in vertical channel. *Journal of Molecular Liquids*, vol. 216, pp. 103-110.

Thripathy, R. S.; Dash, G. C.; Mishra, S. R.; Hoque, M. M. (2016): Numerical analysis of hydromagnetic micropolar fluid along a stretching sheet embedded in porous medium with non-uniform heat source and chemical reaction. *Engineering Science and Technology*, vol. 19, no. 3, pp. 1573-1581.

Thumma, T.; Beg, O. A.; Kadir, A. (2017): Numerical study of heat source/sink effects on dissipative magnetic nanofluid flow from a non-linear inclined stretching/shrinking sheet. *Journal of Molecular Liquids*, vol. 232, pp. 159-173.

Thumma, T.; Beg, O. A.; Siva Reddy, S. (2017): Finite element computation of magnetohydrodynamic nanofluid convection from an oscillating inclined plate with radiative flux, heat source and variable temperature effects. *Proceedings of Mechanical Engineering Part N: Journal of Nanomaterials, Nanoengineering and Nano systems*, vol. 231, no. 4, pp. 179-194.